Transport in Porous Media **54:** 361–376, 2004.

An Improved IMPES Method for Two-Phase Flow in Porous Media

ZHANGXIN CHEN*, GUANREN HUAN and BAOYAN LI
Department of Mathematics, Box 750156, Southern Methodist University, Dallas, TX 75275-0156, U.S.A. e-mails: zchen@mail.smu.edu, huan@golem.math.smu.edu, bli@mail.smu.edu

(Received: 14 November 2002)

Abstract. In this paper we develop and numerically study an improved IMPES method for solving a partial differential coupled system for two-phase flow in a three-dimensional porous medium. This improved method utilizes an adaptive control strategy on the choice of a time step for saturation and takes a much larger time step for pressure than for the saturation. Through a stability analysis and a comparison with a simultaneous solution method, we show that this improved IMPES method is effective and efficient for the numerical simulation of two-phase flow and it is capable of solving two-phase coning problems.

Key words: improved IMPES, two-phase, simultaneous solution, coning problem, stability.

1. Introduction

An IMPES method was originally developed by Sheldon *et al*. (1959) and Stone and Gardner (1961). The basic idea of this classical method for solving a partial differential coupled system for two-phase flow in a porous medium is to separate the computation of pressure from that of saturation. Namely, this coupled system is split into a pressure equation and a saturation equation, and the pressure and saturation equations are solved using implicit and explicit time approximation approaches, respectively. This method is simple to set up and efficient to implement, and requires less computer memory compared with other methods such as a simultaneous solution (SS) method (Douglas *et al*., 1959). It is still widely used in petroleum industry. However, for it to be stable, this classical method requires very small time steps for the saturation. This requirement is prohibitive, particularly for long time integration problems and for small grid block problems such as coning problems.

In our numerical experiments and studies of the classical IMPES method with computational time and stability, we have observed that the implicit computation of pressure takes far more time than the explicit computation of saturation, and the explicit scheme for the saturation is stable only if time steps are sufficiently small. For example, for a water and oil system, the water–oil production ratio (WOR)

*Author for correspondence:

curve oscillates if the time steps are not severely restricted. In the light of the fact that the numerical simulation of two-phase flow is still widely used and the IMPES method is still popular in petroleum industry, it is necessary and important to improve this solution method.

In this paper we develop and numerically study an improved IMPES method for solving a partial differential system for two-phase (e.g. water and oil) flow in a three-dimensional porous medium. Based on the above mentioned observations, together with the fact that the pressure changes less rapidly in time than the saturation in this two-phase flow system, it is appropriate to take a larger time step for the former than for the latter to save computational time. On the other hand, for it to be stable (in particular, to get rid of the oscillation of the WOR), this improved method utilizes an adaptive control strategy on the choice of the time step for saturation. This control strategy is adaptively based on the saturation variation. Through a stability analysis and a comparison with an SS method, we show that our improved IMPES method is effective and efficient for the numerical simulation of two-phase flow and it is capable of solving long time integration and small grid block problems. For a benchmark two-phase coning problem, our numerical experiment shows that this improved IMPES method is stable, efficient, and accurate and is 6.7 times as fast as the SS method. As far as the authors know, the classical IMPES method is not able to solve a two-phase coning problem.

This paper is outlined as follows. In the next section we introduce a two-phase flow model in a three-dimensional porous medium. Then, in the third section we review the classical IMPES method, and in the fourth section we test the stability of this method. In the fifth section, we develop an improved IMPES method for the two-phase flow system. In the sixth section we apply this improved method to the numerical simulation of a two-phase coning problem and compare it with the SS method. Finally, in the last section we conclude with a few remarks.

2. A Two-Phase Flow Model

In this section we review the flow of two incompressible, immiscible fluids in a porous medium $\Omega \subset \Re^3$. The mass balance equation for each of the fluid phases is

$$\phi \frac{\partial(\rho_\alpha s_\alpha)}{\partial t} + \nabla \cdot (\rho_\alpha \mathbf{u}_\alpha) = \rho_\alpha q_\alpha, \quad \alpha = \mathrm{w}, \mathrm{o}, \tag{2.1}$$

where $\alpha = \mathrm{w}$ denotes the wetting phase (e.g. water), $\alpha = \mathrm{o}$ indicates the nonwetting phase (e.g. oil), ϕ is the porosity of the medium, and ρ_α, s_α, $\mathbf{u}_\alpha$, and q_α are, respectively, the density, saturation, volumetric velocity, and external volumetric flow rate of the α-phase. The volumetric velocity $\mathbf{u}_\alpha$ is given by the Darcy law

$$\mathbf{u}_\alpha = -\frac{K_{r\alpha}}{\mu_\alpha}\mathbf{K}\nabla(p_\alpha - \rho_\alpha g Z), \quad \alpha = \mathrm{w}, \mathrm{o}, \tag{2.2}$$

where $\mathbf{K}$ is the absolute permeability of the porous medium, p_α, μ_α, and $K_{r\alpha}$ are the pressure, viscosity, and relative permeability of the α-phase, respectively, g denotes the gravitational constant, Z is the depth, and the z-coordinate is in the vertical downward direction. In addition to (2.1) and (2.2), the constraint for the saturations is

$$s_w + s_o = 1, \tag{2.3}$$

and the two pressures are related by the capillary pressure function

$$p_c(s_w) = p_o - p_w. \tag{2.4}$$

We introduce the phase mobility functions

$$\lambda_\alpha(\mathbf{x}, s_\alpha) = \frac{K_{r\alpha}}{\mu_\alpha}, \quad \alpha = w, o,$$

and the total mobility

$$\lambda(\mathbf{x}, s) = \lambda_w + \lambda_o,$$

where $s = s_w$. The fractional flow functions are defined by

$$f_\alpha(\mathbf{x}, s) = \frac{\lambda_\alpha}{\lambda}, \quad \alpha = w, o.$$

The model is completed by specifying boundary and initial conditions. In this paper we consider no flow boundary conditions

$$\mathbf{u}_\alpha \cdot \boldsymbol{\nu} = 0, \qquad \alpha = w, o, \qquad \mathbf{x} \in \partial\Omega, \tag{2.5}$$

where $\boldsymbol{\nu}$ is the outer unit normal to the boundary $\partial\Omega$ of Ω. The initial condition is given by

$$s(\mathbf{x}, 0) = s_0(\mathbf{x}), \quad \mathbf{x} \in \Omega. \tag{2.6}$$

For a theoretical study of the model in this section, the reader may refer to the paper by Chen (2001), for example.

3. The Classical IMPES Method

We use the oil phase pressure as the pressure variable

$$p = p_o, \tag{3.1}$$

and define the total velocity

$$\mathbf{u} = \mathbf{u}_w + \mathbf{u}_o. \tag{3.2}$$

Under the assumption that the fluids are incompressible, we apply (2.3) and (3.2) to (2.1) to see that

$$\nabla \cdot \mathbf{u} = q(p, s) \equiv q_{\mathrm{w}}(p, s) + q_{\mathrm{o}}(p, s), \tag{3.3}$$

and (2.4) and (3.2) to (2.2) to obtain

$$\mathbf{u} = -\mathbf{K}\left(\lambda(s)\nabla p - \lambda_{\mathrm{w}}(s)\nabla p_{\mathrm{c}} - \left(\lambda_{\mathrm{w}}\rho_{\mathrm{w}} + \lambda_{\mathrm{o}}\rho_{\mathrm{o}}\right)g\nabla Z\right). \tag{3.4}$$

Similarly, apply (2.4), (3.2), and (3.4) to (2.1) and (2.2) with $\alpha = \mathrm{w}$ to have the saturation equation

$$\phi\frac{\partial s}{\partial t} + \nabla \cdot \left\{\mathbf{K}f_{\mathrm{w}}(s)\lambda_{\mathrm{o}}(s)\left(\frac{\mathrm{d}p_{\mathrm{c}}}{\mathrm{d}s}\nabla s + (\rho_{\mathrm{o}} - \rho_{\mathrm{w}})g\nabla Z\right) + f_{\mathrm{w}}(s)\mathbf{u}\right\} = q_{\mathrm{w}}(p, s). \tag{3.5}$$

We substitute (3.4) into (3.3) to give the pressure equation

$$-\nabla \cdot \left(\mathbf{K}\lambda\nabla p\right) = q - \nabla \cdot \left(\mathbf{K}(\lambda_{\mathrm{w}}\nabla p_{\mathrm{c}} + (\lambda_{\mathrm{w}}\rho_{\mathrm{w}} + \lambda_{\mathrm{o}}\rho_{\mathrm{o}})g\nabla Z\right). \tag{3.6}$$

Let $J = (0, T)$ $(T > 0)$ be the time interval of interest, and for a positive integer N, let $0 = t^0 < t^1 < \cdots < t^N = T$ be a partition of J. In the pressure computation in the IMPES method, the saturation s in (3.6) is supposed to be known, and (3.6) is solved implicitly for p. That is, for each $n = 0, 1, \ldots$, p^n satisfies

$$-\nabla \cdot \left(\mathbf{K}\lambda(s^n)\nabla p^n\right) = F(p^n, s^n), \tag{3.7}$$

where $F(p, s)$ denotes the right-hand side of (3.6) and s^n is supposed to be given.

It follows from (3.5) that

$$\phi\frac{\partial s}{\partial t} = q_{\mathrm{w}} - \nabla \cdot \left\{\mathbf{K}f_{\mathrm{w}}(s)\lambda_{\mathrm{o}}(s)\left(\frac{\mathrm{d}p_{\mathrm{c}}}{\mathrm{d}s}\nabla s + (\rho_{\mathrm{o}} - \rho_{\mathrm{w}})g\nabla Z\right) + f_{\mathrm{w}}(s)\mathbf{u}\right\}. \tag{3.8}$$

In this classical IMPES method, (3.8) is explicitly solved for s; that is, for each $n = 0, 1, 2, \ldots$, s^{n+1} satisfies

$$\phi\frac{\partial s^{n+1}}{\partial t} = G(p^n, \mathbf{u}^n, s^n), \tag{3.9}$$

where $G(p, \mathbf{u}, s)$ represents the right-hand side of (3.8).

Now, the standard IMPES method goes as follows: After startup from (2.6), for $n = 0, 1, \ldots$, we use (3.7) and s^n to evaluate p^n and then (3.4) to evaluate $\mathbf{u}^n$; next, we exploit s^n, p^n, $\mathbf{u}^n$, and (3.9) to compute s^{n+1}. As noted, the time step $\Delta t^n = t^n - t^{n-1}$ must be sufficiently small for this method to be stable; see the next section.

4. Numerical Stability Tests

We present numerical experiments of the classical IMPES method with computational time and stability. For this, we define the source and sink terms in (2.1) by

$$q_\alpha = \sum_{l,m} q_\alpha^{l,m} \delta(\mathbf{x} - \mathbf{x}^{l,m}), \quad \alpha = \mathrm{w}, \mathrm{o}, \tag{4.1}$$

where $q_\alpha^{l,m}$ indicates the volume of the fluid produced or injected per unit time at the lth well and the mth perforated zone, $\mathbf{x}^{l,m}$, for phase α and δ is the Dirac delta function. Following Peaceman (1991), $q_\alpha^{l,m}$ can be defined by

$$q_\alpha^{l,m} = \frac{2\pi \bar{K} K_{r\alpha} \Delta L^{l,m}}{\mu_\alpha \ln r_e^l / r_c^l} \left(p_{bh}^l - p_\alpha - \rho_\alpha g (Z_{bh}^l - Z) \right), \tag{4.2}$$

where $\Delta L^{l,m}$ is the length (in the flow direction) of a grid block (containing the lth well) at the mth perforated zone, p_{bh}^l is the flowing bottom hole pressure at the datum level depth Z_{bh}^l, r_e^l is the equivalent well radius, and r_c^l is the radius of the lth well. The quantity $\bar{K}$ is some average of $\mathbf{K}$ at wells (Peaceman, 1991). For a diagonal tensor $\mathbf{K} = \mathrm{diag}\,(K_{11}, K_{11}, K_{33})$, for example, $\bar{K} = K_{11}$ at a vertical well, where K_{11} and K_{33} are the permeabilities in the horizontal and vertical directions, respectively. In this case, the equivalent radius is calculated by

$$r_e^l = 0.14 \left(DX^2 + DY^2 \right)^{1/2}, \tag{4.3}$$

where DX and DY are the x- and y-dimensions of the grid block which contains this vertical well. For a horizontal well (e.g. in the x-direction), $\bar{K} = \sqrt{K_{11} K_{33}}$ and

$$r_e^l = \frac{0.14 \left((K_{33}/K_{11})^{1/2} DX^2 + (K_{11}/K_{33})^{1/2} DZ^2 \right)^{1/2}}{0.5 \left((K_{33}/K_{11})^{1/4} + (K_{11}/K_{33})^{1/4} \right)}, \tag{4.4}$$

where DZ is the z-dimension of the grid block containing this horizontal well.

The physical data used are taken from the paper by Nghiem *et al.* (1991). The reservoir dimensions are

$$\sum_{i=1}^{NX} DX(i), \qquad \sum_{j=1}^{NY} DY(j), \quad \text{and} \quad \sum_{k=1}^{NZ} DZ(k), \tag{4.5}$$

respectively, in the x-, y-, and z-directions, where $NX = 9$, $NY = 9$, $NZ = 6$, and (in feet)

$$\begin{aligned}
DX(i) &= 300, \quad i = 1, 2, \ldots, 9, \\
DY(1) &= DY(9) = 620, \qquad DY(2) = DY(8) = 400, \\
DY(3) &= DY(7) = 200, \qquad DY(4) = DY(6) = 100, \qquad DY(5) = 60, \\
DZ(1) &= DZ(2) = DZ(3) = DZ(4) = 20, \\
DZ(5) &= 30, \qquad DZ(6) = 50.
\end{aligned} \tag{4.6}$$

A horizontal oil production well is located in the first layer ($k = 1$) and stretched in grid blocks with $i = 6, 7, 8$ and $j = 5$, and a horizontal water injection well is located in the sixth layer ($k = 6$) and stretched in grid blocks with $i = 1, 2, \ldots, 9$ and $j = 5$. Thus we have two wells in this experiment: a horizontal production well and a horizontal injection well. The radius of both wells is 2.25 in. The permeability tensor $\mathbf{K}$ is diagonal with $K_{11} = 300$ md and $K_{33} = 30$ md, and the porosity ϕ is 0.2. The depth Z of the centers of the six layers is, respectively, 3600, 3620, 3640, 3660, 3685, and 3725 ft, and the initial water saturation at each layer is 0.289, 0.348, 0.473, 0.649, 0.869, and 1. The densities and viscosities are $\rho_o = 0.8975\,\text{g/cm}^3$, $\rho_w = 0.9814\,\text{g/cm}^3$, $\mu_o = 0.954$ cp, and $\mu_w = 0.96$ cp. The relative permeability and capillary pressure data are shown in Table I.

Table I. The relative permeability and capillary pressure data

s	0.22	0.3	0.4	0.5	0.6	0.8	0.9	1
K_{rw}	0	0.07	0.15	0.24	0.33	0.65	0.83	1
K_{ro}	1	0.4	0.125	0.0649	0.0048	0	0	0
p_c	6.3	3.6	2.7	2.25	1.8	0.9	0.45	0.0

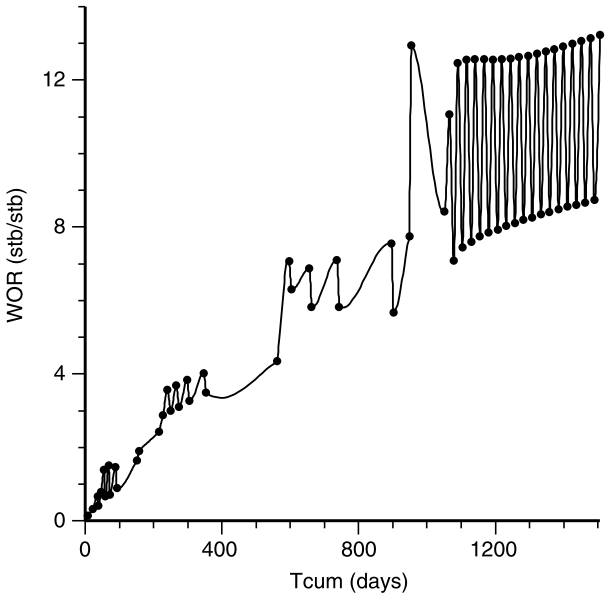

Figure 1. Water–oil ratio versus time. $DS_{max} = 0.05$.

Finally, the pressure at the wells is fixed, the datum level depth Z_{bh} is 3600 ft, and the bottom hole pressures p_{bh} for the injection and production wells are, 3651.4 and 3513.6 psi, respectively. In the following calculations, the final time T is 1500 days.

As noted, to control the variation of saturation, we need to find a suitable time step Δt^{n+1} before we solve Equation (3.9) for s^{n+1} for each $n = 0, 1, \ldots$ The control strategy is defined as follows: We calculate the maximum value of $\partial s^{n+1}/\partial t$

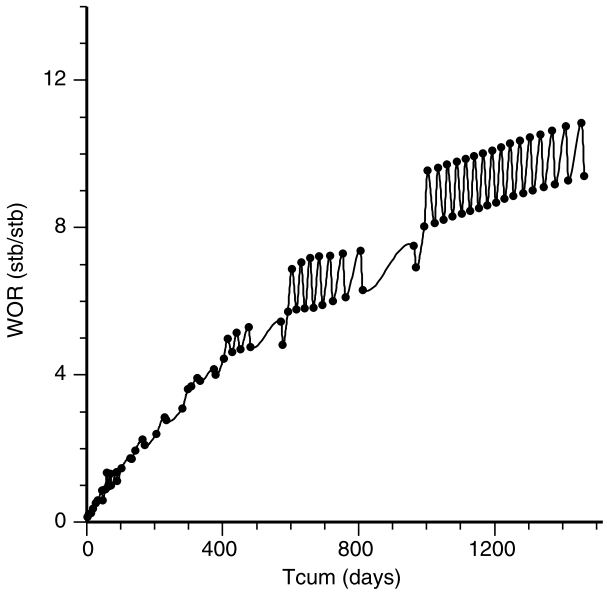

Figure 2. Water–oil ratio versus time. $DS_{\max} = 0.02$.

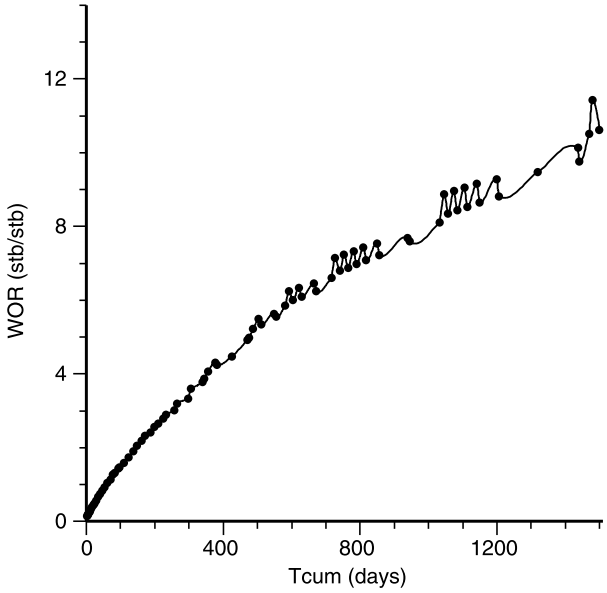

Figure 3. Water–oil ratio versus time. $DS_{\max} = 0.01$.

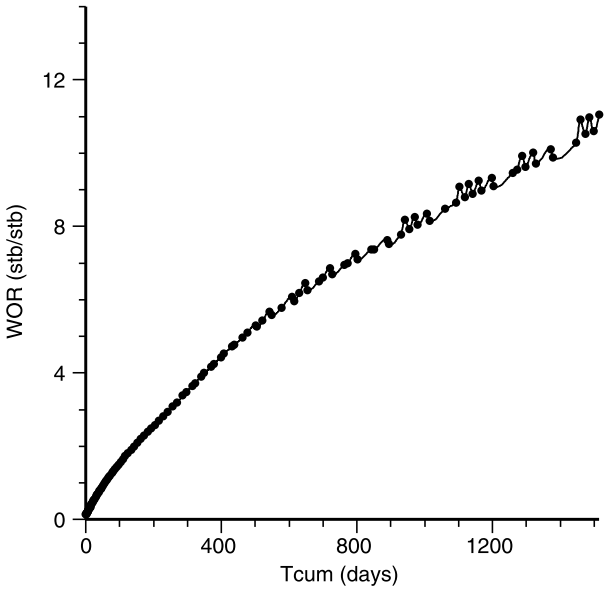

Figure 4. Water–oil ratio versus time. $DS_{\max} = 0.005$.

at all computational nodes, denoted by $\left(\partial s^{n+1}/\partial t\right)_{\max}$, which is, by (3.9),

$$\left(\frac{\partial s^{n+1}}{\partial t}\right)_{\max} = \left(\frac{G(p^n, \mathbf{u}^n, s^n)}{\phi}\right)_{\max}. \tag{4.7}$$

Then we apply the following formula to find Δt^{n+1}:

$$\Delta t^{n+1} = \frac{DS_{\max}}{(\partial s^{n+1}/\partial t)_{\max}}, \tag{4.8}$$

where $DS_{\max}$ is the maximum variation of the saturation to allow. Now, we use this time step in (3.9) to obtain s^{n+1}. This approach guarantees that the saturation variation does not exceed $DS_{\max}$. Note that $DS_{\max}$ can depend on the time level n.

The numerical method used is based on a seven-point block-centered finite difference method with harmonic averaged coefficients (equivalently, a mixed finite element method (Russell and Wheeler, 1983)) in three dimensions. To test stability, we study the curves of the WOR at the production well versus time (days) in the cases of $DS_{\max} = 0.05$, 0.02, 0.01, 0.005, 0.002, and 0.001. The results are displayed in Figures 1–6. From these figures we see that WOR does not oscillate only when $DS_{\max}$ is smaller than 0.002.

We now check the computational time for the present experiment at $T = 1500$ days for the six choices of $DS_{\max}$, which is shown in Table II. In this table, the CPU time is in second and N (the number of time steps) is such that $t^N = T$. All the computations are carried out on an SGI-O_2 workstation. Table II shows that the computation of pressure takes far more time than that of saturation. For example,

in the case of $DS_{\max} = 0.002$, the CPU time for the former is 47.68 s, while it is 0.46 s for the latter. Thus in this case the difference is 100 times more.

In summary, from the above stability analysis and CPU time study we conclude that (1) WOR is stable only when $DS_{\max}$ is smaller than 0.002, (2) the total CPU

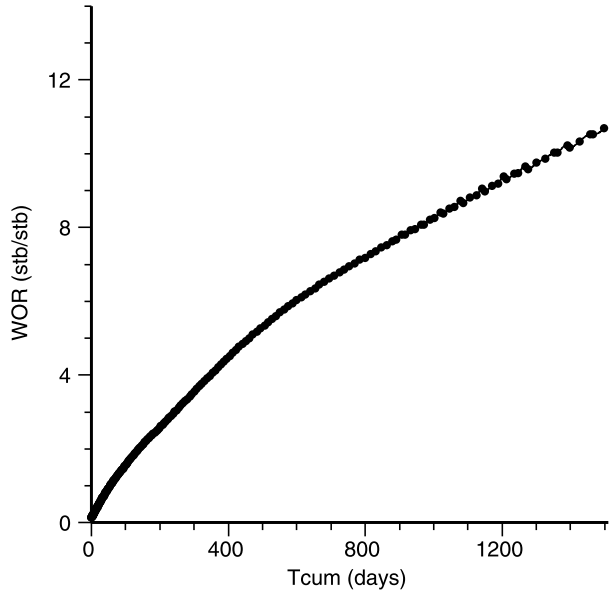

Figure 5. Water–oil ratio versus time. $DS_{\max} = 0.002$.

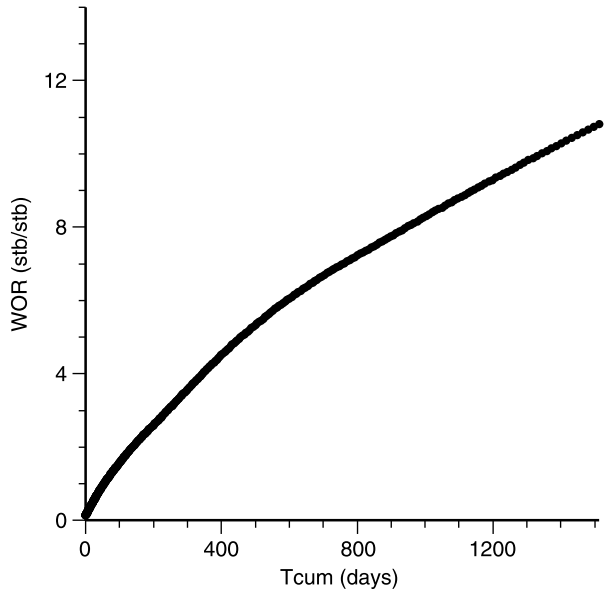

Figure 6. Water–oil ratio versus time. $DS_{\max} = 0.001$.

Table II. The CPU time versus $DS_{\max}$

$DS_{\max}$	0.05	0.02	0.01	0.005	0.002	0.001
N	70	91	86	122	226	432
Pressure-CPU	14.81	19.18	18.13	25.86	47.68	89.49
Saturation-CPU	0.14	0.20	0.19	0.35	0.46	0.88

time almost doubles as $DS_{\max}$ decreases, and (3) most of the CPU time is spent on the pressure computation.

5. An Improved IMPES Method

5.1. THE IMPROVED METHOD

As discussed in the previous sections, most of the computational time in the classical IMPES method is spent on the implicit calculation of the pressure. Also, it follows from the mechanics of fluid flow in porous media that the pressure changes less rapidly in time than the saturation. Furthermore, the constraint for time steps is primarily used for the explicit calculation of the saturation. For all these reasons, it is appropriate to take a much larger time step for the pressure than for the saturation.

Again, for a positive integer N, let $0 = t^0 < t^1 < \cdots < t^N = T$ be a partition of J for the pressure into subintervals $J^n = (t^{n-1}, t^n)$, with length $\Delta t_p^n = t^n - t^{n-1}$. Each subinterval J^n is divided into sub-subintervals $J^{n,m} = (t^{n-1,m-1}, t^{n-1,m})$ for the saturation:

$$t^{n-1,m} = t^{n-1} + \frac{m\Delta t_p^n}{M^n}, \quad m = 1, \ldots, M^n.$$

The length of $J^{n,m}$ is denoted by $\Delta t_s^{n,m} = t^{n-1,m} - t^{n-1,m-1}$, $m = 1, \ldots, M^n$, $n = 0, 1, \ldots$ The number of steps, M^n, can depend on n. Below we simply write $t^{n-1,0} = t^{n-1}$, and set $v^{n,m} = v(\cdot, t^{n,m})$.

We denote the right-hand side of (3.4) by $\mathbf{H}(p, s)$. Now, the improved IMPES method is defined as follows: For each $n = 0, 1, \ldots$, find p^n such that

$$-\nabla \cdot \left(\mathbf{K}\lambda(s^n)\nabla p^n\right) = F(p^n, s^n), \tag{5.1}$$

and $\mathbf{u}^n$ such that

$$\mathbf{u}^n = \mathbf{H}(p^n, s^n). \tag{5.2}$$

Next, for $m = 1, \ldots, M^n$, $n = 0, 1, \ldots$, find $s^{n+1,m}$ such that

$$\phi \frac{\partial s^{n+1,m}}{\partial t} = G(p^n, \mathbf{u}^n, s^{n+1,m-1}). \tag{5.3}$$

The time step $\Delta t_s^{n+1,m}$ in (5.3) is chosen as follows: Set

$$\left(\frac{\partial s^{n+1,m}}{\partial t}\right)_{\max} = \left(\frac{G(p^n, \mathbf{u}^n, s^{n+1,m-1})}{\phi}\right)_{\max}, \tag{5.4}$$

and then calculate

$$\Delta t_s^{n+1,m} = \frac{DS_{\max}}{(\partial s^{n+1,m}/\partial t)_{\max}}, \quad m = 1, \ldots, M^n, \ n = 0, 1, \ldots \tag{5.5}$$

5.2. NUMERICAL TESTS

We now perform a numerical experiment with the improved IMPES method for the same example as in the fourth section. The selection of pressure time steps is automatic, and the total variation of the saturation for one pressure time step is fixed at 0.05. We test three values of $DS_{\max}$ for the choice of $\Delta t_s^{n+1,m}$, $m = 1, \ldots, M^n$, $n = 0, 1, \ldots$ The numerical results are illustrated in Table III, and the WOR curves for these three values are shown in Figure 7, where the final time is such that the calculated water cut is up to 98% at the production well.

From Figure 7, we see that the WOR curves slightly oscillate when $DS_{\max} = 0.01$ and 0.005, and this curve is very smooth when $DS_{\max} = 0.001$. From Table III, the total CPU times as $DS_{\max} = 0.001$ is 2.73 s. Also, the ratio of the pressure CPU time to the saturation CPU time is around 1.8:1. This is in sharp contrast with the classical IMPES method where the total CPU time doubles as $DS_{\max}$ decreases and the pressure CPU is 100 times as much as the saturation CPU. Furthermore, the total CPU time for the improved IMPES is far less than that for the classical one. For example, as $DS_{\max} = 0.001$, the former is 2.73 s and the latter is 90.37.

5.3. A COMPARISON WITH SS

To see further the accuracy and efficiency of the improved IMPES method, we compare it with the SS method for the same numerical example. Here the pressure time step is fixed at 100 days, $DS_{\max} = 0.001$, and the final time is 1500 days. The daily oil production rate (versus time), the cumulative oil production, and the WOR

Table III. The CPU time for the improved IMPES

$DS_{\max}$	$M \equiv M^n$	N	Pres-CPU	Satur-CPU	Total CPU
0.01	5	18	3.63	0.28	3.91
0.005	10	12	2.38	0.33	2.71
0.001	50	9	1.76	0.97	2.73

curve using these two methods are presented in Figures 8–10. These curves match very well for these two methods. The total CPU time for the improved IMPES is 5.03 s, while it is 31.58 s for the SS. Thus, for this example, the improved IMPES is 6.3 times as fast as the SS.

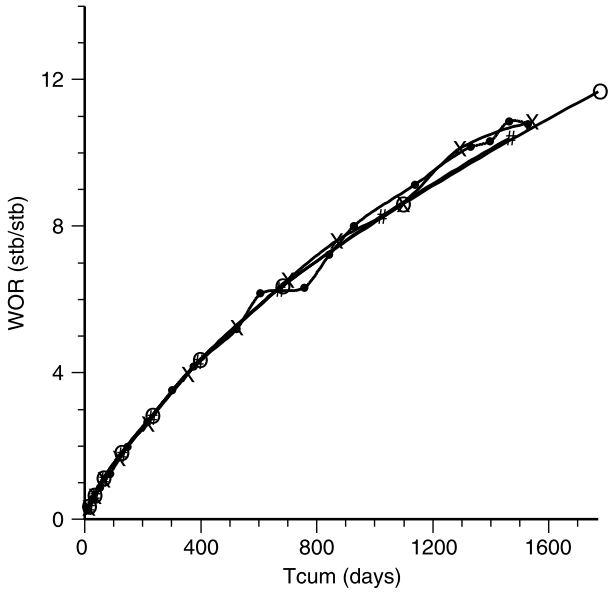

Figure 7. Water–oil ratio versus time. × = 0.05, • = 0.01, ○ = 0.001.

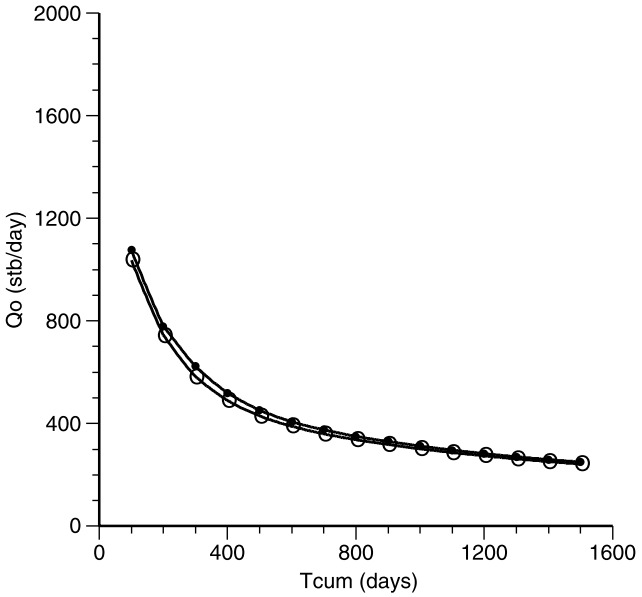

Figure 8. Oil production versus time for case 1a. ○ = IMPES, • = SS.

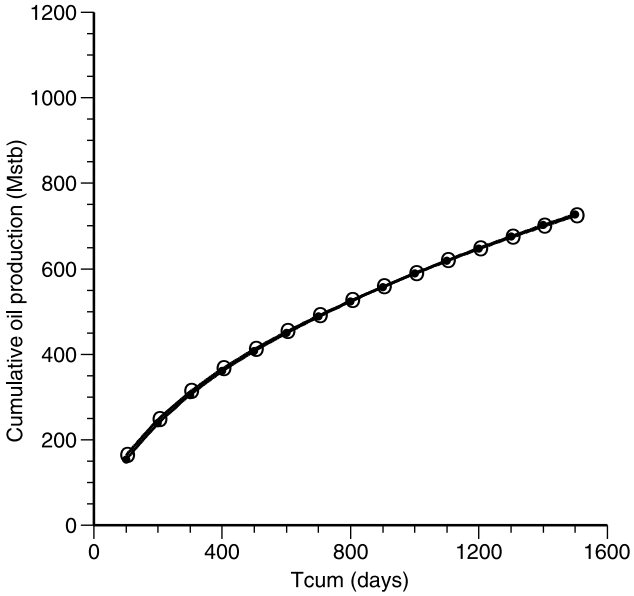

Figure 9. Cumulative oil prod. versus time for case 1a. ○ = IMPES, ● = SS.

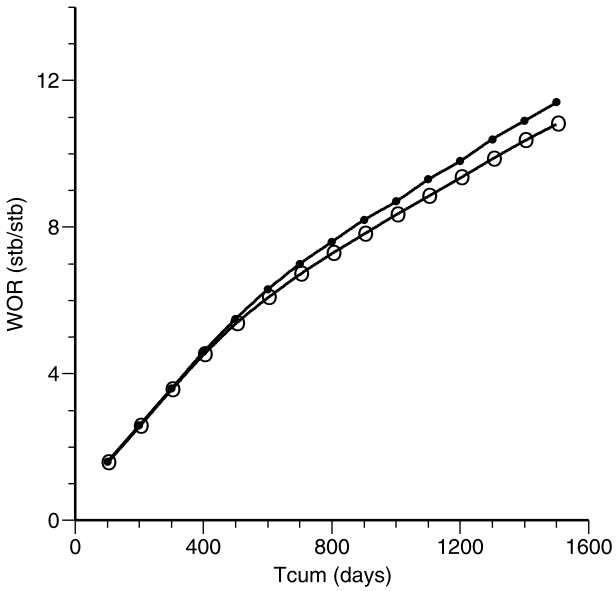

Figure 10. Water–oil ratio versus time for case 1a. ○ = IMPES, ● = SS.

6. Application to a Coning Problem

As far as the authors know, the classical IMPES method has not successfully been applied to the solution of a two-phase coning problem. In the final section, to check

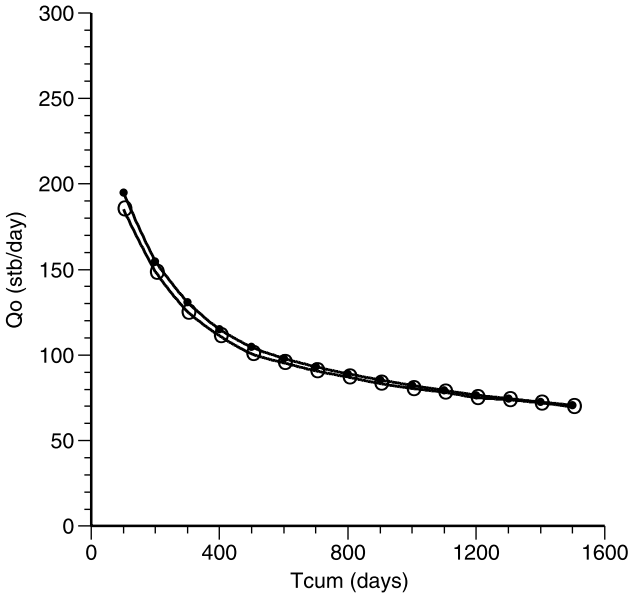

Figure 11. Oil production versus time for model 2. ○ = IMPES, • = SS.

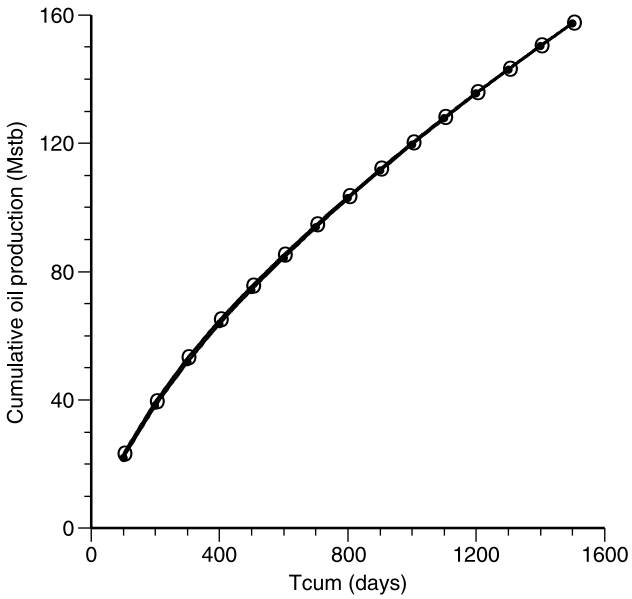

Figure 12. Cumulative oil production versus time for model 2. ○ = IMPES, • = SS.

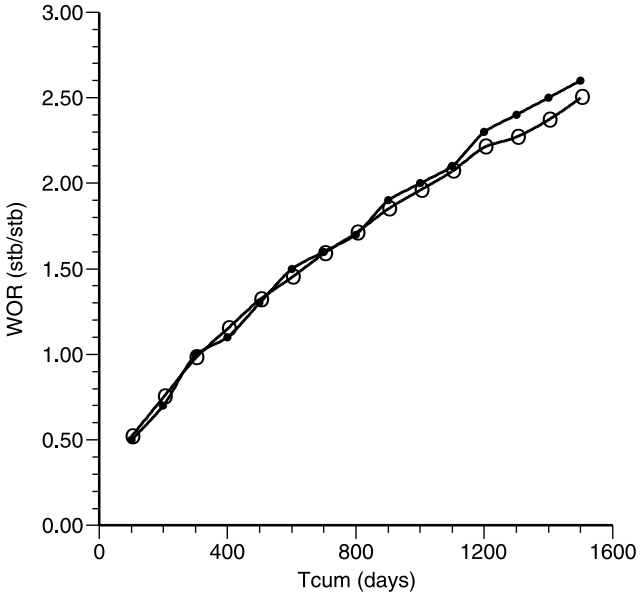

Figure 13. Water–oil ratio versus time for model 2. ○ = IMPES, ● = SS.

its robustness, we apply the improved IMPES method to solve a problem of this type. Now, the reservoir is a cylindrical domain with its axis parallel to the z-axis and its radius equal to 1343.43 ft. There are two vertical wells located at the center of the reservoir: An oil production well vertically sits in the first layer and a water injection well in the sixth layer. The radii of the innermost to outermost cylinders are, respectively, 4, 8, 16, 32, 64, 128, 256, 512, and 1343.43 ft. All other data are the same as in the first example in the previous sections. The pressure and saturation time steps are as in Section 5.3. For the present problem, the daily oil production rate, the cumulative oil production, and the WOR curve using the improved IMPES and SS methods are presented in Figures 11–13. Again, these curves match quite well for these two methods. The total CPU time for the former is 2.54 s, and for the latter is 17.02 s. Hence this improved IMPES is 6.7 times as fast as the SS for the present coning problem. Also, we point out that the pressure CPU time is 0.39 s, while the saturation CPU time is 2.15 s. From this experiment, we see that the improved IMPES method is capable of solving two-phase coning problems.

7. Concluding Remarks

Based on numerical stability and computational time analyses, in this paper we have developed an improved IMPES method for the numerical simulation of two-phase flow in porous media. Through comparisons with the classical IMPES and SS methods, we have showed that this improved method is stable, efficient, and accurate, and it is capable of solving two-phase coning problems. We will investigate

the application of this method to other models of fluid flow in porous media such as the black-oil and compositional models.

Acknowledgements

This work is supported in part by National Science Foundation grants DMS-9972147 and INT-9901498 and by a gift grant from the Mobil Technology Company.

References

Chen, Z.: 2001, Degenerate two-phase incompressible flow: Existence, uniqueness and regularity of a weak solution, *J. Differ. Equations* **171**, 203–232.

Douglas Jr., J., Peaceman, D. W. and Rachford Jr., H. H.: 1959, A method for calculating multi-dimensional immiscible displacement, *T. SPE AIME* **216**, 297–306.

Nghiem, L. S., Collins, D. A. and Sharma, R.: 1991, Seventh SPE comparative solution project: Modeling of horizontal wells in reservoir simulation, in: *SPE 21221, 11th SPE Symposium on Reservoir Simulation in Anaheim*, California, 17–20 February 1991.

Peaceman, D. W.: 1991, Presentation of a horizontal well in numerical reservoir simulation, in: SPE 21217, *11th SPE Symposium on Reservoir Simulation in Ananheim*, California, 17–20 Febuary 1991.

Russell, T. and Wheeler, M. F.: 1983, Finite element and finite difference methods for continuous flows in porous media, Chapter II, The mathematics of reservoir simulation, in: R. Ewing (ed.), *Frontiers in Applied Mathematics 1*, Society for Industrial and Applied Mathematics, Philadelphia, pp. 35–106.

Sheldon, J. W., Zondek, B. and Cardwell, W. T.: 1959, One-dimensional, incompressible, non-capillary, two-phase fluid flow in a porous medium, *T. SPE AIME* **216**, 290–296.

Stone, H. L. and Garder Jr., A. O.: 1961, Analysis of gas-cap or dissolved-gas reservoirs, *T. SPE AIME* **222**, 92–104.